Pure appl. geophys. 159 (2002) 221–245
0033–4553/02/030221–25 $ 1.50 + 0.20/0

Pure and Applied Geophysics

Simulation of Unstable Fault Slip in Granite Using a Bonded-particle Model

JAMES F. HAZZARD,[1] DAVID S. COLLINS,[2]
WILLIAM S. PETTITT,[2] and R. PAUL YOUNG[1]

Abstract—A bonded-particle model is used to simulate shear-type microseismic events induced by tunnel excavation in granite. The model represents a volume of granite by an assembly of 50,000 individual particles bonded together at points of contact. A plane of weakness is included in the model and this plane is subjected to increasing shear load while the normal load across the plane is held constant. As shear stress in the model increases, bonds begin to break and small acoustic emissions (AE) result. After enough bonds have broken, macro-slip occurs across the large portions of the fault in an unstable manner. Since the model is run dynamically, seismic source information can be calculated for the simulated AE and macro-slip events. This information is compared with actual results obtained from seismic monitoring around an underground excavation. Although the modelled events exhibit larger magnitudes than the actual recorded events, there are many similarities between the model and the actual results, namely the presence of foreshocks before the macro-slip events and the patterns of energy release during loading. In particular, the model provides the ability to examine the complexity of the slip events in detail.

Key words: Numerical modelling, PFC, source complexity, acoustic emissions, microcrack, dynamic triggering.

Introduction

Unstable stick-slip motion commonly observed in the frictional sliding of rock was first proposed as a mechanism for earthquakes by BRACE and BYERLEE (1966). Since then, many experiments have been conducted to map out the conditions that cause unstable sliding and therefore earthquakes. It has been found that the factors controlling the stability of slip are quite complex and involve a variety of possible micromechanisms such as interlocking, riding up and shearing of asperities (see SCHOLZ, 1990).

Recently the increase in computer power has enabled the creation of full micromechanical/discontinuum numerical models to examine the mechanics involved

[1] Department of Earth Sciences, University of Liverpool, 4 Brownlow St., Liverpool, L69 7GP, U.K.
E-mail: hazzard@liv.ac.uk
[2] Applied Seismology Consultants, 10 Belmont, Shrewsbury, Shropshire, SY1 1TE, U.K.
E-mail: dave@seismology.org

with earthquakes and faulting. ANTONELLINI and POLLARD (1995) use the distinct element method to examine the formation of deformation bands in sandstone. In their work, the sand grains are represented by cylindrical elements that move independently of one another and they show that shear localisation occurs along discrete faults when external stresses are applied. MORGAN and BOETTCHER (1999) conduct similar experiments and examine the effects of grain size distribution and interparticle friction on the mechanics of localisation. The particle-based lattice solid model is used by MORA and PLACE (1998) to simulate earthquakes with gouge and to endeavor to explain the heat flow paradox, and distinct element models are used by SCOTT (1996) to explore the same issues. Finally CUNDALL (1999) uses a bonded particle model to explore the behaviour of rough joints in shear. All of these studies have contributed greatly to understanding the mechanisms of shear slip, however none have considered the dynamic effects, i.e., waves emitted when unstable slip occurs and how this released energy could be used to calculate seismic source information, and how these waves might affect the model behaviour.

The work presented here uses discontinuum models to simulate a microseismic event recorded near an underground excavation to provide insight into the complexities of unstable shear slip, and endeavor to explain the observed seismic results. A bonded particle model is used (ITASCA CONSULTING GROUP, 1999) so that cracking and faulting can occur spontaneously throughout the model. Individual cracks can form between model elements and these cracks are then able to coalesce into larger fractures or faults. In addition, the model is run dynamically so that each crack releases seismic energy and actual source magnitudes and mechanisms can be obtained.

Seismicity on Different Scales

Relationships between earthquakes of different sizes and magnitudes have been intensely studied with the intention of formulating scaling relationships (see SCHOLZ, 1990, pp. 180–189 for a summary). Due to the large range in earthquake magnitudes (>10 orders of magnitude) it is difficult to compare different sized earthquakes because of the need for different measurement techniques and instrumentation. One avenue that shows considerable promise is the investigation of mining-scale microseismic events. Examining these small earthquakes is useful because of the well-constrained environment, the ability to directly observe the earthquake sources (e.g., slabbing around a tunnel) and the possibility of direct comparison with large well-controlled laboratory tests (e.g., MCGARR, 1994). An experiment in which microseismic events are monitored on two different scales is described in COLLINS *et al.* (this issue – hereafter referred to as COLLINS *et al.*, 2002) and that experiment is the basis for the numerical modelling presented in this paper (see below for a summary).

In the microseismic monitoring experiment (COLLINS *et al.*, 2002), many tiny foreshocks and aftershocks were recorded prior to, and following the microseismic

events. It is proposed that by studying the locations and mechanics of the foreshocks, a better understanding of stress evolution leading up to the main shock could be obtained, and this may contribute to the long-term goal of large-scale earthquake prediction. By examining the locations and mechanisms of all of the recorded events, it was postulated that the foreshocks represent crack opening or the shearing and breaking of asperities along the eventual main-shock fracture plane, and that the aftershocks are small slip episodes that occur as the fracture restabilises. By reproducing these experiments with numerical models, it is hoped that further insight can be gained into the mechanics of unstable shear faulting, and that the models can be partially validated by comparison with the actual information obtained from the underground experiment.

Acoustic Emissions and Microseismic Events at the URL

Two scales of seismic monitoring are presently being performed simultaneously around a tunnel excavation in the Tunnel Sealing eXperiment (TSX) at Atomic Energy of Canada Ltd.'s Underground Research Laboratory (URL), Canada. Small scale, high frequency AEs (frequency range 30–300 kHz) are being recorded in a $10 \times 10 \times 10$ m volume using a 16-channel ultrasonic array (COLLINS and YOUNG, 1998) Three-dimensional source locations and full moment tensor analyses have been performed for many of these events to observe the AE source mechanisms (PETTITT, 1998).

The TSX tunnel is also one of a network of tunnels at the URL that is being monitored by a lower frequency (0.1–10 kHz) microseismic (MS) array covering a $100 \times 100 \times 100$ m volume (COLLINS and YOUNG, 2000). This combination of monitoring the same rock mass using both microseismic and ultrasonic techniques affords the unique ability to investigate fracturing over different magnitude scales. The combined AE and MS systems record seismicity with moment magnitudes between -7 and -2, with only a small magnitude gap where the systems have non-overlapping monitoring frequencies. Of particular interest here is the observation by COLLINS and YOUNG (1998) that AEs are locating in very tight spatial and temporal clusters around the TSX tunnel consisting of often ten or more events. Each AE cluster can be associated in both time and space with one or more microseismic hypocentres. Detailed analyses of these AE/MS clusters are described in COLLINS *et al.* (2002).

One cluster of seismicity recorded during the TSX experiment was chosen for numerical simulation. The cluster is made up of 86 AEs spanning a volume of approximately $50 \times 25 \times 25$ cm close to the floor of the TSX tunnel (Cluster 2 in COLLINS *et al.*, 2002). Associated with the AEs are two larger microseismic (MS) events that occurred within the time and space of the AE cluster (see Fig. 1). The MS mechanisms suggest that these events represent shear slip on a failure plane oriented parallel to the tunnel perimeter.

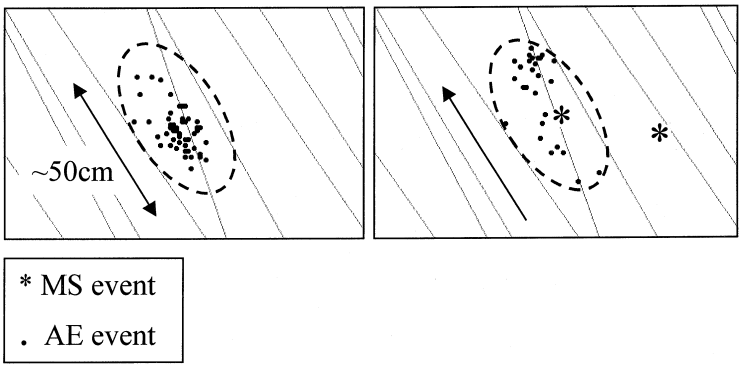

Figure 1
Plan views showing (left) the AE events which occur before the time of the MS events, and (right) the AE events which occur during and after the MS events. The arrow in the right plot denotes the direction of temporal AE migration. The thin grey lines have no physical meaning – they represent the construction lines of the 3-D CAD drawing of the tunnel on which the events are superimposed. (from COLLINS *et al.*, 2002).

Bonded Particle Models

Itasca Consulting Group's Particle Flow Code in Two Dimensions (PFC^{2D}) is used to numerically simulate a small volume of rock near the TSX tunnel. This code represents rock as a dense packing of circular particles (disks) with some random size distribution. The particles are assumed to be rigid (non-deformable), however overlap can occur at particle contacts (see Fig. 2). Contacts are assumed to exist only at a point and not over some finite surface area as would be the case with fully deformable particles. Particles are bonded together at points of contact to simulate a competent rock (rather than an assembly of grains).

Each contact can be envisaged as a pair of elastic springs with constant normal and shear stiffness. Each 'spring' also has a normal and shear strength that can be exceeded, causing the connecting bond to break. The normal force at a contact is given by:

$$\begin{aligned} &\text{Bond intact}: \quad F_i^n = K^n U^n n_i \\ &\text{Bond broken}: \quad F_i^n = K^n U^n n_i \quad U^n > 0 \\ &\qquad\qquad\qquad\quad F_i^n = 0 \qquad\quad U^n < 0 \end{aligned} \tag{1}$$

where K^n is the normal stiffness of the contact, U^n is the amount of overlap (positive is compression and negative is tension), and n_i is the unit normal vector to the contact (see Fig. 2). The contact bond has infinite compressional strength although the tensile strength is finite. If the tensile force at the contact exceeds the tensile strength, then the bond breaks and the contact normal force becomes zero.

The shear force can be calculated in a similar way however when the shear strength of the bond is exceeded and the bond breaks, the shear force does not drop

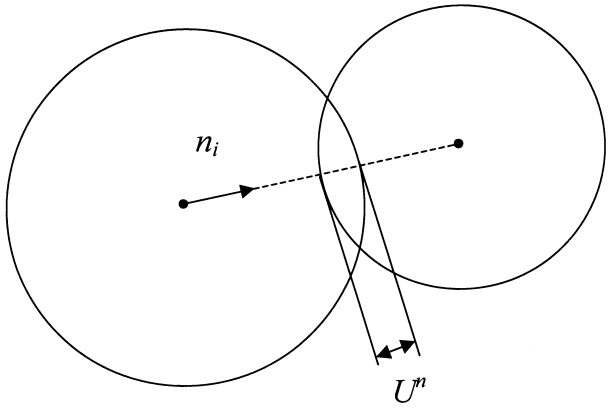

Figure 2
Ball–ball contact in PFC^{2D}.

to zero but instead frictional sliding takes over. The maximum shear force that can be supported at a contact is therefore given by:

$$\begin{aligned} &\text{Bond intact:} \quad F^s_{\max} = \text{ shear bond strength} \\ &\text{Bond broken:} \quad F^s_{\max} = \mu \left| F^n_i \right| \end{aligned} \tag{2}$$

where μ is the coefficient of friction between the two particles. The shear contact behaviour can be thought of as possessing cohesion while the bond is intact and then becomes frictional after the bond breaks. The values of contact normal and shear stiffness and bond normal and shear strength are specified by the user and these values influence the overall stiffness (modulus) and strength of the modelled rock sample, respectively.

From the contact forces, particle accelerations can be calculated according to Newton's law of motion and from the accelerations, new particle positions can be obtained after each time step. The distinct element method (CUNDALL and STRACK, 1979) is employed to model the forces and motions of the particles within the assembly. This technique assumes that information cannot propagate further than a nearest neighbour in one calculation step. Therefore time steps are very small and many of them are required to reach equilibrium. This method is identical to that used in explicit finite-difference analyses and allows information to propagate dynamically through the system. For this reason, PFC^{2D} is a logical choice for modelling acoustic emissions and the resulting dynamic output.

In PFC, when the tensile or shear bond strength at a contact is exceeded and the bond breaks, contact forces drop instantaneously. A more realistic contact behaviour could be incorporated in which failure occurs over finite time, however this was not done for the models described here. Similarly, stress-corrosion or subcritical crack growth could be accounted for by making the strength of the bonds time and stress-

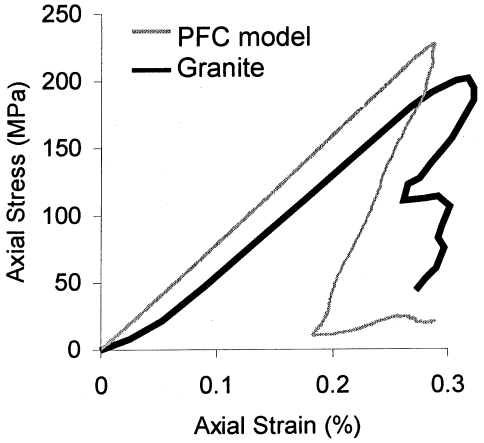

Figure 3
Comparison between the mechanical behaviour of a PFC model and an actual sample of Lac du Bonnet granite subjected to a uniaxial compression test.

dependent (see POTYONDY and CUNDALL, 1998), however for simplicity this was also not considered here.

Since particle micro-parameters cannot be determined directly, estimated values for the particle stiffnesses and bond strengths were assigned and uniaxial compression tests were simulated to determine the macro-strength and stiffness of the material. The micro-properties were then adjusted until the model reproduced the approximate stiffness and strength of Lac du Bonnet granite (see HAZZARD *et al.*, 2000). Note that the particle micro-stiffnesses are constant throughout the model but the bond strengths were assigned a Poisson's distribution about a mean value with a standard deviation of 25%. This ensured a more gradual sample failure with cracking occurring over a longer period of time than would be the case if all bonds were assigned the same strength. Figure 3 shows the mechanical behaviour of PFC model of a core sample ($\sim$8000 particles) during a uniaxial compression test compared with a laboratory test on a sample of Lac du Bonnet granite. The stiffness and strength of the material are well reproduced by the model. Note however that the initial curvature of the stress/strain curve is missing in the model. This is because there are no pre-existing cracks in the model that can close under stress. The effects of the different microparameters and particle packings on the macro-behaviour of PFC models have been thoroughly examined elsewhere (POTYONDY and CUNDALL, 1999) and will not be explored here. Further descriptions of bonded particle models and justification for their use in modelling competent rocks is given in HAZZARD *et al.* (2000).

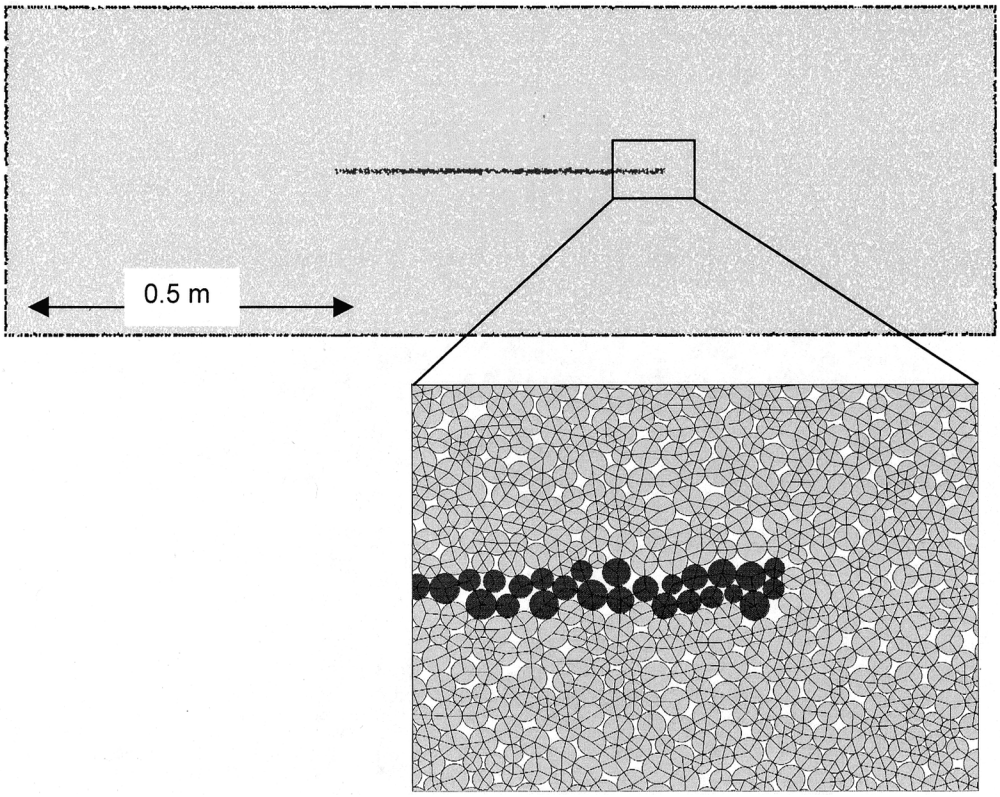

Figure 4
PFC^{2D} model of "shear box". Contact bonds are shown as black lines. Particles with three or more weakened bonds are darkened.

Simulation of Shear Fault

The shear-slip event was numerically simulated by creating a "shear box" model in PFC^{2D}. The box represents a $1.5 \times 0.5 \times 0.25$ m block of Lac du Bonnet granite with a 50 cm long plane of weakness in the centre corresponding to the extent of the recorded seismicity (see Fig. 4). The long axis of the model (and therefore the plane of weakness) is assumed to be parallel to the tunnel perimeter. The model comprises approximately 50,000 particles randomly placed within the rectangle (see Fig. 4). Note that because this is a 2-D simulation, the particles are actually disks or cylinders. The particle diameters range from 3 to 5 mm which is approximately the size of the grains in the granite. The particles (disks) are assigned thicknesses of 0.25 m so that the width of the fault zone is approximately the same as that measured for the actual microseismic event as described above.

The plane of weakness is simulated by weakening all bonds within 1 maximum particle diameter (5 mm) of the centre line. The strengths of these bonds were set to 10% of the bond strengths in the surrounding rock. The assumption of a weak fault is thought to be valid since many studies on tectonic-scale faults have shown faults to be significantly weaker than the surrounding rock. The specific value of 10% chosen for this modelled fault is somewhat arbitrary, however it can be shown that altering the strength between 10% and 50% of the surrounding rock strength has no major impact on the results. If the fault strength is set considerably weaker than 10% then stable sliding results. It is assumed that the weak bonds connecting particles on opposite sides of the fault represent interlocking asperities or weakly bonded fault segments. The bonds within 0.5 m of the left and right edges were not weakened to the end that the model simulates a fault of finite length embedded in a homogeneous rock mass.

Note that if bonds on the fault were assigned zero strength then the fault still exhibits inherent roughness. Shear resistance develops as interlocking particles ride up to move past each other. If zero strength and zero friction are assigned to the fault particles and the fault is extended to the sample edges, then a fault friction angle of 30° results. This suggests that fault roughness can be simulated without bonding (cohesion) on the fault, however when this was done the shear sliding was found to be stable (no stress drop) and therefore of little seismic interest. The minor episodes of energy release that result from particles jumping over one another could be considered tiny acoustic emissions, however this was not considered here.

The normal force across the plane of weakness was assumed to be 5 MPa. This value was determined by observing the minimum stress at the AE locations from a boundary element model of the TSX tunnel. For all of the AE, the minimum stress was less than 5 MPa and oriented approximately perpendicular to the tunnel perimeter. In the PFC model, this normal force is maintained by a servo-mechanism acting on the top layer of particles.

The shear force is increased from zero by applying a constant velocity to the boundary particles in the top half of the model. A velocity of 0.05 m/s was applied. This is about 5 orders of magnitude slower than the *P*-wave velocity of the material being modelled consequently it is assumed that this loading velocity is slow enough to prevent any dynamic effects (i.e., a wave propagating from the moving boundaries). The boundary particles in the lower half of the model are held fixed.

These boundary conditions are probably more representative of a laboratory shear box test than an actual *in situ* simulation. *In situ*, it is likely that the normal force will increase as the fault dilates (low compliance for normal motion) and the shear stress will be approximately constant instead of increasing monotonically. The "shear-box" boundary conditions are used here because slight cracking or slip would occur on the fault if the shear stress was held constant, unless some time-dependent stress-corrosion mechanism was included. As described above, this mechanism has not yet been implemented.

The microparameters (contact stiffness and strength) are chosen, based on previous PFC^{2D} models of Lac du Bonnet granite (POTYONDY *et al.*, 1996). The chosen micro-parameters cause the bonded particle assembly to exhibit approximately the same macro-strength and stiffness as actual Lac du Bonnet granite (see Fig. 3).

Results

Microseismic Events

The average shear stress on the fault is plotted against the average shear displacement across the fault in Figure 5. These values were obtained by taking the average of five stress and strain measurements at evenly spaced positions along the fault. The inset of Figure 5 shows the average shear slip plotted against time. The time has been normalised by dividing by T, the time taken for a compressional wave to propagate horizontally across the entire model. This normalisation technique was proposed by MORA and PLACE (1998) because the rate at which the stress is applied in the model must be unrealistically fast due to the small time-steps required. By

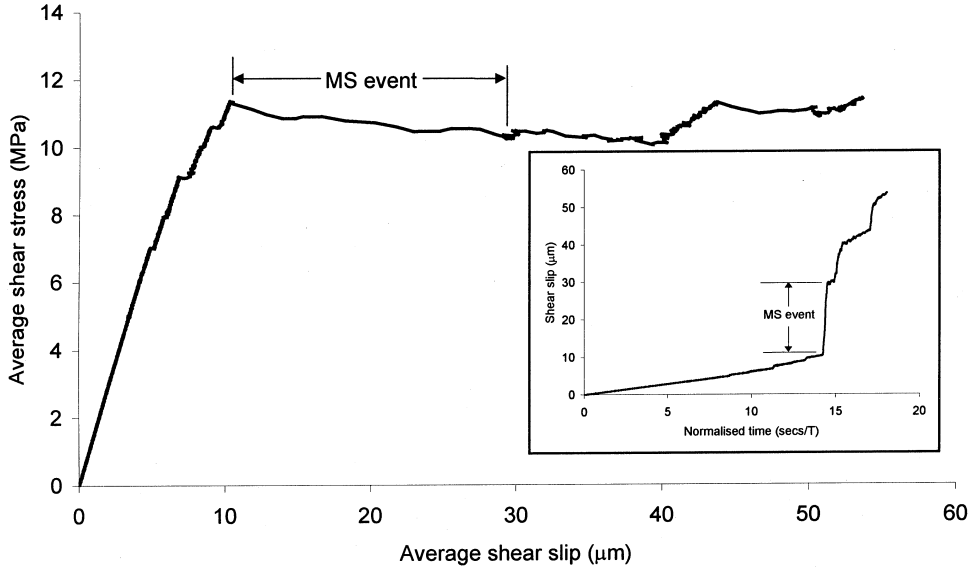

Figure 5
Stress/strain behaviour of the modelled fault. The inset shows the average shear slip plotted against time. The time has been normalised by dividing by T, the time taken for a compressional wave to propagate horizontally across the entire model.

normalising the time a more reasonable time scale results, similar to loading rates *in situ*.

Figure 5 shows the shear stress initially increasing in a linear fashion with only a slight increase in shear displacement. Since the fault is assumed to be "locked" initially, this displacement is attributed to elastic deformation and a few small cracks that occur before the major slip event. When the stress reaches about 11 MPa, rapid slip then occurs, accompanied by a drop in stress. This region represents unstable sliding and is accompanied by a jump in kinetic energy in the model – just as for an actual earthquake. This earthquake is assumed to correspond to the first MS event recorded at the actual TSX tunnel as described above.

The seismic moment of the modelled MS event can be calculated by:

$$M_0 = \mu DA \ , \tag{3}$$

where μ is the shear modulus of the rock, D is the shear slip and A is the fault area. The shear modulus was determined experimentally to be 25.5 GPa (near the actual value for Lac du Bonnet granite of 27.4 GPa), the fault slip was determined from Figure 5 to be 19.2 μm and the fault area is 0.125 m^2 (i.e., 0.5 m long $\times$ 0.25 m thick). This yields a value of $M_0 = 6.12 \times 10^4$ Nm. The moment magnitude can then be calculated by:

$$M_w = \frac{2}{3}\log M_0 - 6.0 \ . \tag{4}$$

This yields a magnitude of $M_w = -2.8$ for this event. This value is about an order of magnitude greater than that observed for the first MS recorded in the actual TSX experiment ($M_w = -3.9$). There are several possible reasons for this and these will be considered in the discussion section.

Figure 5 delineates that the first episode of slip is rapidly followed by another slightly smaller slip event. The magnitude of this event can be calculated as above, yielding a moment magnitude for this second event of $M_w = -3.0$. Comparing this to the magnitude of the second MS event recorded for this cluster at the TSX ($M_w = -3.7$), it can be seen again that the model produces a magnitude almost an order of magnitude larger than the actual event. A comparison of the seismicity obtained from the model and the seismicity recorded at the TSX is presented in Table 1.

If the modelled particle assembly continues to be loaded in shear, more slip events occur with decreasing magnitudes as the fault plane weakens (through more bond breakages) and approaches stable sliding conditions (see Fig. 5). For the events recorded at the TSX it is unlikely that a continual application of shear stress was present, therefore the model was stopped at some arbitrary time after the occurrence of a few events. Since only 2 MS events were recorded at the TSX, only the first two slip events produced by the model will be considered here.

Table 1

Comparison of modelled and actual seismicity

Event	Model magnitude	Actual magnitude
MS 1	−2.8	−3.9
MS 2	−3.0	−3.7
AE	−5.3 to −3.1 (78 events)	−6.9 to −5.4 (86 events)

Microcracks

During loading, many bond breakages occur in the PFC model. Each of these bond breakages may be considered an individual microcrack (HAZZARD *et al.*, 2000). The location, mechanism and orientation of the microcracks that form before, during and after the MS event are shown in Figure 6. Crack orientations are normal to the line connecting the centres of the two parent particles. The mode of failure for each

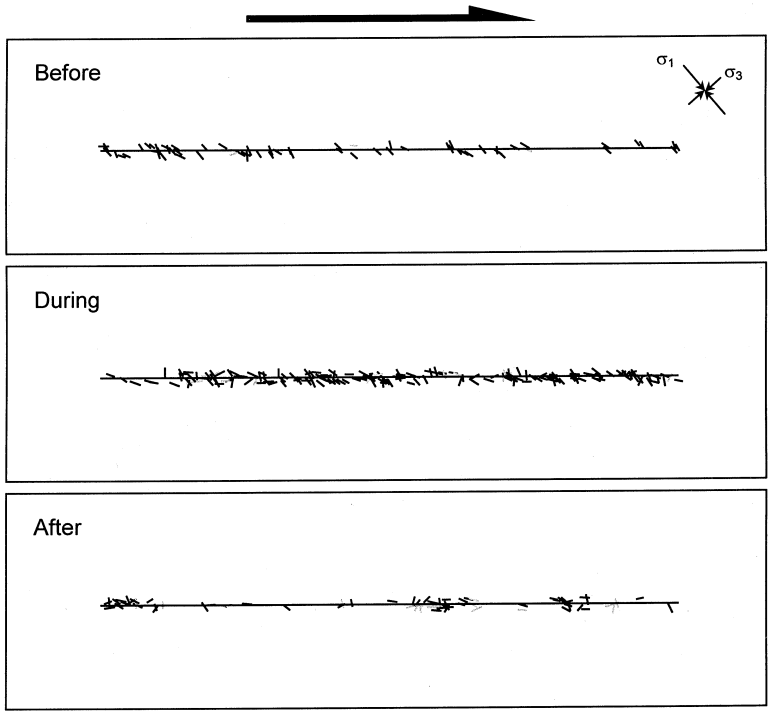

Figure 6

A close-up of the fault zone (the extent of which is indicated by a thin horizontal line) showing microcracks forming before, during and after the microseismic event. Tensile cracks are black and shear cracks are grey. The direction of shear is shown at the top. The principal stresses at the centre of the model just prior to the MS event are shown in the top right corner.

crack corresponds to whether the tensile or shear strength of the contact bond was exceeded.

It can be seen that the majority of cracks in all plots are tensile and are oriented approximately 45° to 50° clockwise from the orientation of the fault. These microcracks therefore correspond to tensile cracks opening in the direction of least principal stress, σ_3 and oriented parallel to the maximum stress, σ_1 (see Fig. 6). The mechanism of cracking agrees with what is generally observed in compression tests on intact crystalline rocks (TAPPONIER and BRACE, 1976). It is of interest that these tensile cracks contribute to unstable shear slip on the fault (the MS event). This will be addressed in the discussion section.

Figure 6 shows that before the MS event the cracking is comparatively sparse and the cracks locate rather evenly along the length of the fault. It is proposed that these cracks represent the foreshocks to the MS event(s) and help weaken parts of the fault to facilitate shear slip. It is also possible that these bond breakages shed stress to intact parts of the fault (concentrating stress on stronger asperities), bringing the system closer to macro-failure conditions.

During the first MS event there is considerably more cracking along the entire fault length. These cracks are obviously associated with the MS event, and it will be shown later that there is a somewhat complicated relationship between the microcracks and the shear slip on the fault. After the first MS event the cracks form in small, distinct clusters indicating where further small slip events are occurring (aftershocks). It is interesting to note that the orientations of the cracks which occur after the MS event are generally more parallel to the fault than the orientations of the foreshock cracks.

Acoustic Emissions

If a PFC model is run dynamically with low numerical damping, each time a bond breaks, the stored strain energy at the contact is released as kinetic energy in the form of seismic waves. In this model the numerical damping was set such that the rock has a seismic quality factor, Q, of approximately 100. Q is a common measure of attenuation or energy loss in real rocks and is defined as 2π times the ratio of stored energy to dissipated energy in one wavelength. FEUSTEL (1995) calculates the quality factor of Lac du Bonnet granite to be approximately 220. However, since the simulation presented here is close to a tunnel where much stress-relief cracking is thought to have occurred, then a lower value of $Q = 100$ is assumed.

Because this is a simulation of a fairly competent rock, and Q is quite high, there is very little loss in wave amplitude across the length of the model due to attenuation ($\sim$5%). If geometrical spreading is considered then a wave's amplitude will decrease by about 90% across the model. This presents the problem that waves may be reflected off the boundaries. In this model no attempt is made to simulate absorbing boundaries. A non-absorbing boundary may be realistic for one side of

the model that is thought to represent the surface of the tunnel, however, this condition is unrealistic for the rest of the model in which the rock extends indefinitely away from the fault. The effect of these reflecting boundaries is that excessive energy is present in the system and more events with larger magnitudes may be occurring than would be the case for absorbing boundaries. Further study is required to formulate more realistic boundary conditions for dynamic models in PFC.

Previous work has shown that realistic seismic information can only be obtained from the PFC-generated cracks if they are clustered together into larger "events". If each crack is considered individually then all events will exhibit approximately the same magnitude. Therefore it is assumed that cracks occurring very close together in space and time make up one single acoustic emission. The criteria used to cluster the cracks into AEs and the way in which seismic information is obtained from the modelled AEs are described by HAZZARD and YOUNG (2000). This algorithm basically assumes that an AE is a small rupture propagating at 0.5 times the shear-wave velocity of the material. When a microcrack forms, the kinetic energy of all particles within a distance of three-particle diameters from the crack location is monitored. The kinetic energy of the source particles is monitored for the length of time it would take for a shear rupture to propagate from the microcrack location (the centre of the source) to the edge of the source ($time = (3\ particle\ diameters)/(0.5\times$ shear-wave velocity)). If another crack forms within the source area during this time then it is considered part of the same seismic event. The source area is then expanded to include all particles within three diameters of the new crack. When no more cracks form within the source area, the AE magnitude is calculated from the peak kinetic energy attained by the particles in the source region over the duration of the event. In this way, microcracks occurring close together in space and time are considered part of the same rupturing event and a larger range of AE magnitudes is therefore possible.

When this AE recording technique is applied to the PFC model described here, a total of 78 AE are observed with magnitudes ranging from −5.3 to −3.1. This is roughly the same number of AE recorded in the actual TSX experiment (86), however the number of AE recorded in the PFC model will of course depend on how long the model is run and the clustering criteria used. To test the effect of the clustering criteria, the model was rerun with different clustering parameters. Two additional tests were run in which the initial source radius was set to one and two particle diameters. Figure 7 shows the magnitude distribution for the events when the initial source radius is set to one particle diameter and for the case when the initial source radius is set to three diameters (the case for two diameters is not shown for clarity but it falls in between the two plots shown). It can be seen that for smaller initial source areas less cracks are clustered and therefore there are more small magnitude events. The slopes of the straight part of the curves correspond to the Gutenberg-Richter b value, which is a quantitative indication of the magnitude

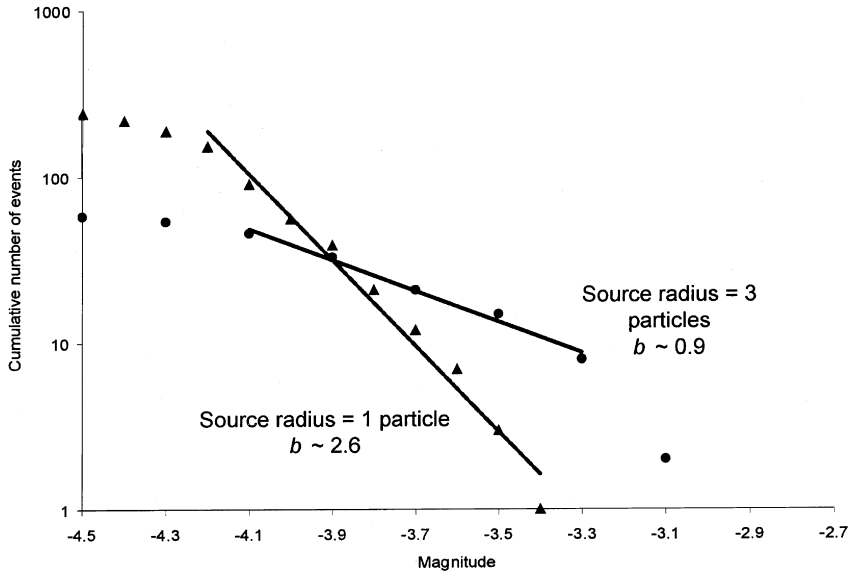

Figure 7
Distribution of event magnitudes for AE recorded in PFC model. Plots are shown for two different cases of crack clustering: 1. Initial source radius equals one particle diameter. 2. The initial source radius is three-particle diameters. The slope of the straight part of the curves is the Gutenberg-Richter *b* value.

distribution of events. In studies on actual earthquake series the *b* value is generally close to unity (LOCKNER, 1993). It can be seen from Figure 7 that using an initial source radius of 3 particle diameters provides the most realistic magnitude distribution, therefore only these simulations will be discussed further.

The magnitudes of the AE obtained from PFC are about an order of magnitude larger than those obtained from the actual experiment (see Table 1). One reason for this may be that there is a gap in the range of magnitudes that can be recorded at the TSX (due to the non-overlapping monitoring frequencies of the two systems) therefore events with magnitudes between −5 and −4 are not detected at the TSX. Other possible reasons for the magnitude discrepancy are outlined in the discussion.

The AEs are plotted in Figure 8. In this plot, AEs consisting of more than 2 microcracks are plotted as ellipses and the orientation and size of the ellipses are calculated from the positions of the cracks involved in the AEs. As expected, Figure 8 shows many small AEs occurring prior to the MS and then a few very large AEs occurring during the MS. After the MS the AEs are again quite small. It is interesting that the middle plot of Figure 8 (during the MS) shows that the MS event is actually made up of a few separate AEs instead of just one large event, indicating several separate episodes of cracking and/or slip constitute the actual MS event. This observation is not unrealistic, as it is known that many tectonic-scale earthquakes are

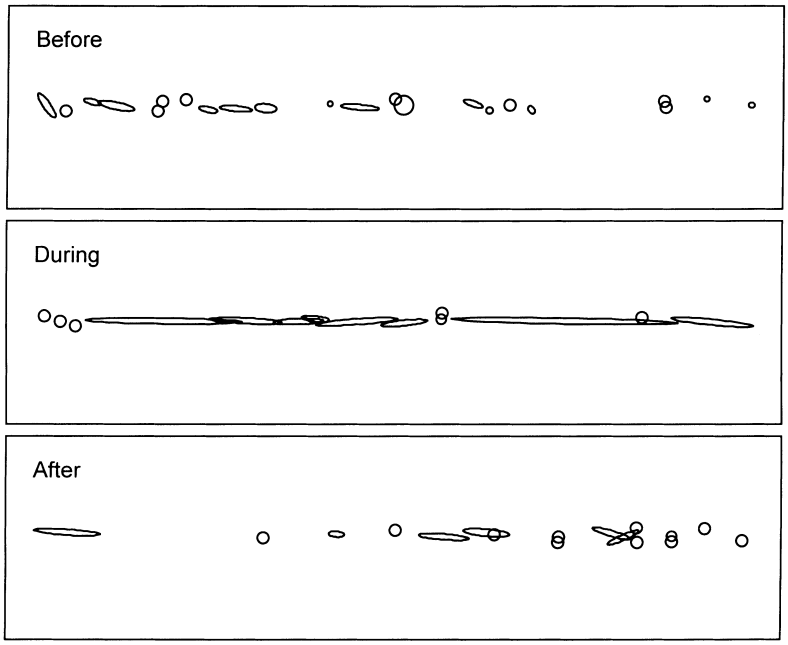

Figure 8
AEs measured in the PFC model before, during and after the first MS event. AEs consisting of more than two cracks are plotted as best-fit ellipses where the ellipse extent and orientation is determined from the locations of the microcracks making up the AE. The extent of the fault is not shown but it extends almost the width of the plots.

often made up of several pulses of slip or rupture (R. Abercrombie, personal communication). It is possible that these separate AEs could be attributed to the incorrect application of the crack clustering algorithm (i.e., if a larger initial source area was used, then more cracks would be clustered and only one large AE would result), however a close examination of the cracking on the fault during the MS reveals several distinct clusters of cracking spaced apart in time and space (see the figures in the discussion section), which indicates the interpretation of several small ruptures is correct.

In all three plots in Figure 8 it appears that the ellipses are generally oriented sub-parallel to the fault zone (and approximately parallel to the direction of maximum shear stress) contrasting with the individual cracks that were oriented approximately 50° to the fault (parallel to σ_1). It appears likely therefore that even though these events are generally composed of several small tensile cracks, the overall mechanism of the events, when motion is averaged over many particles, is probably shear (or some more complex source type). This agrees with the actual TSX results in which the majority of AE showed double-couple mechanisms with the failure plane oriented parallel to the tunnel perimeter.

Triggering

Previous work has shown that when PFC models are run dynamically with low numerical damping, waves emitted from one crack are capable of dynamically triggering more cracks (HAZZARD *et al.*, 2000). This mechanism is observed when a contact bond is stressed such that it is close to its maximum strength. If a transient (dynamic) stress pulse then passes by (caused by a nearby bond breakage) it may be sufficient to cause the contact bond to break. It can be shown that the dynamic stress pulse is often larger and more extensive than the long-term static change in stress caused by a bond breakage.

Figure 9 shows particle velocities and cracking after the start of localisation (after the peak stress in Fig. 5). This figure shows how cracking starts near the right edge of the fault and these cracks cause waves to propagate outwards. Further cracking along the fault then appears to occur as the wavefront passes by, suggesting that the wave may be dynamically triggering cracking on the fault. To investigate this further, the normal forces at some contacts were recorded before and after crack formation.

Figure 10 shows the normal force at a contact where a tensile crack forms. The bond is fixed to prevent breaking so that the total history of normal force at the contact can be observed. It is clear that the passing of a wave would cause the bond to break in this case and that the long-term (static) change in stress would be unlikely to cause bond breakage. Note however that in reality, the strength at a given contact may be frequency dependent. It has been shown that low stresses maintained for a sustained period can cause failure in granite samples and that if stresses are only applied for a short time then substantially higher magnitude stress changes are required to cause failure (see LOCKNER, 1998; SCHMIDTKE and LAJTAI, 1985). No consideration of this effect is made here and it is likely that if the bond strengths were assigned frequency dependence then the dynamic triggering effect would be diminished.

Discussion

It is clear that the shear failure of this simulated fault is very complex. Shear slip is preceded by the formation of many tensile microcracks that weaken the fault such that shearing can occur between unbonded grains. There appear to be three scales of seismicity occurring in this simulation: 1) tiny tensile microcracks oriented parallel to σ_1, 2) small AE oriented sub-parallel to the fault plane with magnitudes ranging from -5.3 to -3.1 and 3) the MS events of magnitudes > -3 representing slip on large portions of the fault. It is proposed that the AEs modelled here correspond to the AEs recorded in the actual experiment. This assumption is made because the AEs recorded in the experiment generally exhibit double-couple source mechanisms with failure planes oriented parallel to the failure plane of the MS event. Few tensile AEs were recorded in the *in situ* experiment, suggesting that the small opening events

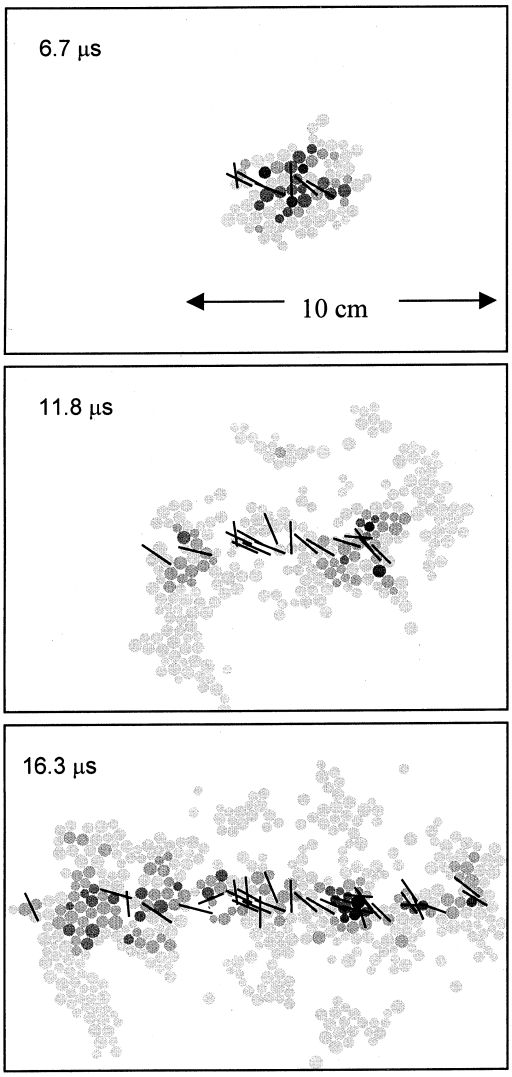

Figure 9
Three frames from a movie showing the velocity of particles and formation of cracks after the peak stress on a small portion of the fault. The shade of the particles indicates the magnitude of the velocity up to a maximum of 4 m/s (black). The time from the peak stress is shown in each frame. The crack sizes are exaggerated 2.5 times.

produced by the PFC model (microcracks) are too small to be picked up by the monitoring equipment. This interpretation is supported by observing that in laboratory AE experiments less than 1% of new microcracks result in recorded AE events (LOCKNER, 1993). Therefore it is possible that the small tensile cracks

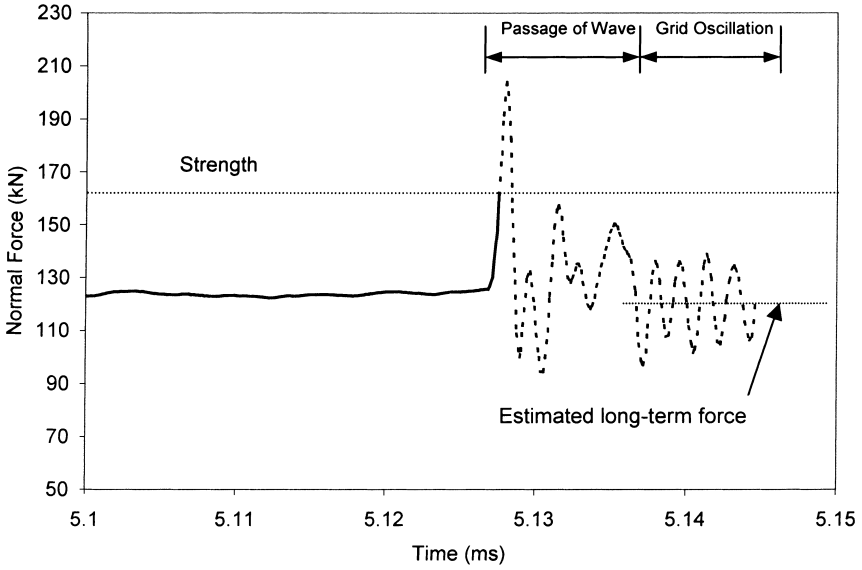

Figure 10
The normal force at a contact close to another bond breakage (tensile is positive). Since the force would normally drop to zero when the bond strength is exceeded, the bond was prevented from breaking so that the contact behaviour could be observed after the strength is exceeded (heavy dashed line).

generated by the PFC model equate to the large number of microcracks that form in rock without emitting detectable acoustic waves.

Another type of 'event' that occurs in the PFC models that has not been discussed is the small bumping and rolling of the round grains required to accommodate shear motion. Since the fault has inherent roughness (friction $\sim 30°$) then energy is required for shear motion to occur. As grains ride over other grains and then drop down again, small amounts of kinetic energy are released. These tiny energy bursts have not been quantified in this study, mostly because they will be much smaller than the events caused by bond breakages, however the observation of these small events would be a very interesting topic for future study.

This simulation shows other similarities with the actual recorded data. AEs are observed in the model before the MS event (foreshocks) and after the MS event (aftershocks) just as in the TSX experiment. The cumulative kinetic energy of the AE events is plotted against normalised time in Figure 11a. The cumulative moments for the actual recorded AEs are shown for comparison (Figure 11b). There are obvious similarities between the two graphs. There are initially a few low energy AEs that occur over a relatively prolonged period prior to the MS events. The number of AEs and the energy released by them then accelerates rapidly just prior to the MS events. The MS in both plots are accompanied by a few high energy (high moment) AEs occurring in rapid succession. The number of AEs and the

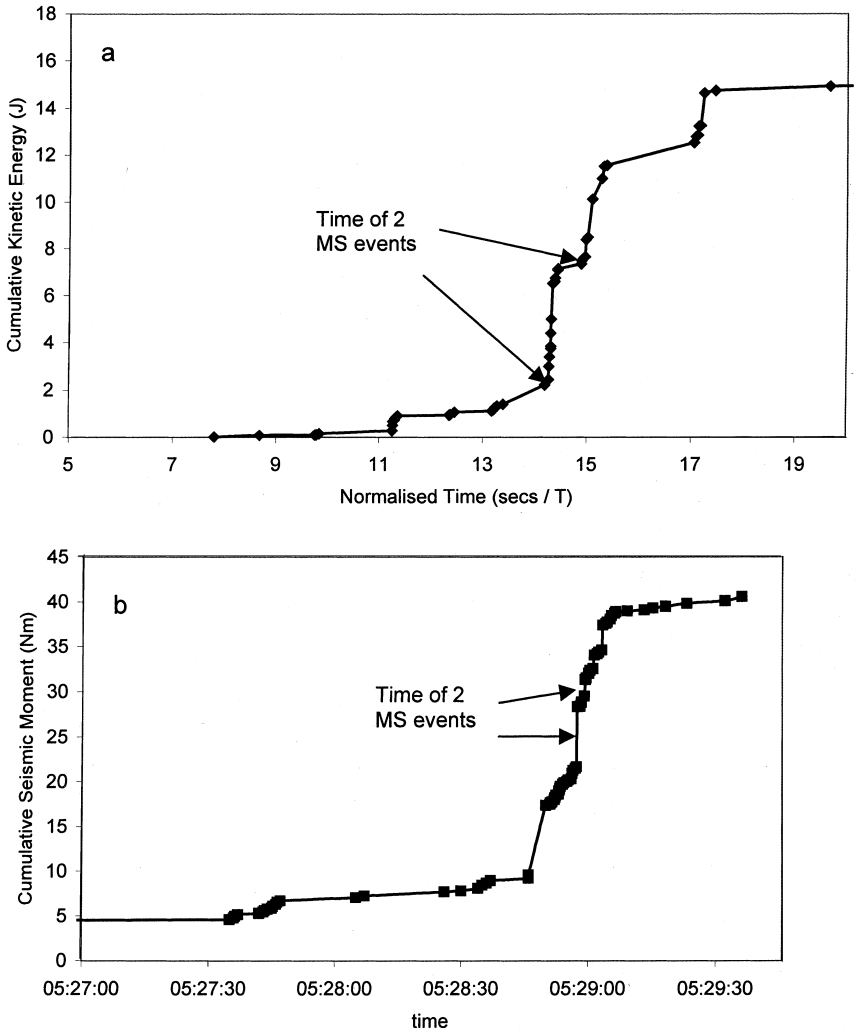

Figure 11
(a) Cumulative energy for all of the AE from the PFC model plotted against normalised time (as in Fig. 5). (b) Cumulative seismic moment for most of the AE recorded for cluster 2 from the TSX experiment (from COLLINS *et al.*, 2002).

energy released by them then decreases again following the two MS events. Note that for the modelled AEs, further AE clusters (associated with episodes of slip – see Fig. 5) continue to occur after the first two MS events because of the continued shear loading of the particle assembly. This continued loading is probably not present in the actual TSX experiment so these subsequent slip events are not observed. Note also that the time scales in Figures 11a and 11b do not correspond directly. This is because the small calculation time steps required by the model

preclude the possibility of extending the seismic activity over minutes or hours as is observed in reality.

The relationships between the foreshocks and main shocks observed in Figure 11 agree qualitatively with what is observed in actual earthquake zones (see BREHM and BRAILE, 1998). The presence of the foreshocks before the main shocks and the accelerating nature of energy release may provide a clue in the pursuit of earthquake prediction. It is therefore encouraging that the numerical model presented here is capable of reproducing the foreshock activity observed in reality. DAS and SCHOLZ (1981) suggest that foreshock activity does not occur for homogeneous fault zones, therefore it is only through the use of numerical models with some type of random fault zone heterogeneity that the observed foreshock patterns can be simulated (e.g., random distribution of bond strengths and random particle packings in PFC).

One difference between the modelled seismicity and the actual recorded seismicity is that the modelled events exhibit magnitudes about an order of magnitude larger than the corresponding events recorded at the TSX. There are several possible reasons for this: (1) the standard seismological equations for calculating magnitude assuming a shear source are not applicable in this case where the source is quite complex, (2) slip is not occurring over the entire fault surface, (3) not enough energy is dissipated by the model, (4) the model is not a sufficiently accurate representation of the processes that are actually occurring. These issues will now be addressed in turn.

1 and 2. Reasons 1 and 2 are related because they both refer to the possible complexity of slip motion on the fault. The complexity of the modelled event can be seen in Figure 9 which shows that cracking during the MS event starts near the edge of the fault and propagates along the fault, perhaps with the help of some dynamic triggering mechanism. To examine how this cracking influences the slip history of the fault, four frames of a movie are shown in Figure 12. These frames show how shear slip starts at a single point on the fault and propagates outwards, following in the wake of the tensile cracking. Therefore it appears that cracking must occur before slip can take place between the unbonded grains. This figure also depicts how slip does not occur along the entire fault simultaneously and that the shearing actually propagates along the fault over some finite amount of time. The propagating nature of the modelled event agrees with the observation made in the actual experiment that the AE locations tend to migrate with time along the fault plane (the direction of the arrow in Fig. 1 indicates the temporal movement of the recorded AE). These observations suggest that our use of equations (3) and (4) to calculate the event magnitude may not be totally appropriate since they assume that slip occurs on the entire fault surface simultaneously. A more rigorous time-dependent method may be required to achieve truly accurate results (see BAKER and YOUNG, 1997).

3. Previous work by the authors (unpublished) has shown that seismic events in PFC are generally too efficient. MCGARR (1994) suggests that the efficiency of seismic events should be less than about 5% (where efficiency is the ratio of radiated energy

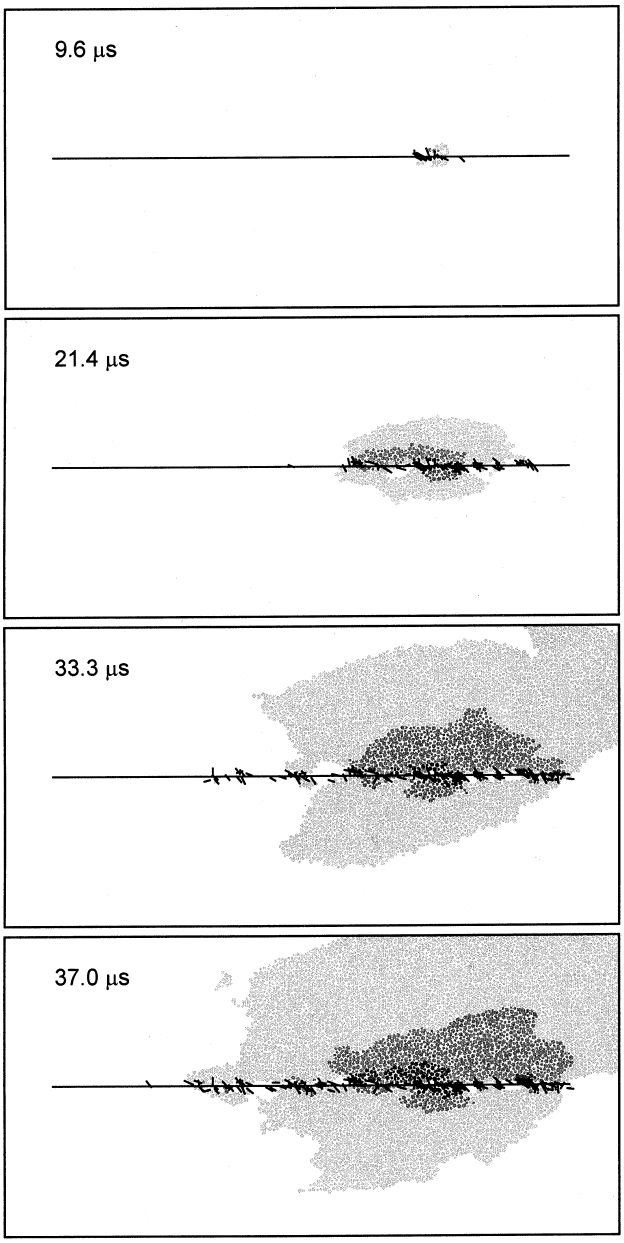

Figure 12
Horizontal displacements of particles from the time of peak stress (absolute value). The shade of the particles indicates the magnitude of displacement up to a maximum of 15 μm (black). Time since the peak stress is shown in each frame.

to total released energy). In the granite model presented here with a realistic amount of numerical damping (to account for wave attenuation) efficiencies approach 50%. This is likely because no energy loss occurs directly due to crack formation (i.e., fracture energy). When a bond breaks, all of the strain energy stored at a contact is converted into kinetic energy or dissipated through interparticle friction and numerical damping. Also, no gouge material exists and therefore insufficient energy dissipates in the breaking of asperities to form gouge and through frictional heating of gouge particles. Another possibility is that some of the kinetic energy used to calculate the AE magnitudes may actually be "incoherent" energy representing jostling and rolling of grains, and that not all of this energy would be radiated in a coherent way such that it could be recorded on a distant receiver (P. Cundall, personal communication). Means to account for these increased efficiencies in PFC are being investigated.

4. COLLINS *et al.* (2002) suggest that the event they recorded may actually be "triggered" instead of induced. This conclusion is drawn by observing that the event occurred approximately four months after the tunnel excavation (the major stress change). This suggests that the event we are considering was caused by a very small change in stress or pore pressure, and processes such as time-dependent creep and stress corrosion may be contributing to the rock failure. In contrast, the event in the PFC model was caused by a direct application of stress. COLLINS *et al.* (2002) show that an "induced" event occurring a few hours after excavation exhibits a considerably larger magnitude (−2.1). The processes causing this event may be closer to the processes simulated with PFC, which would explain why the PFC event magnitude is so large. Future models will endeavor to more accurately simulate the actual conditions by maintaining a constant shear stress across the fault and then subjecting the modelled rock to stress corrosion until failure occurs (see POTYONDY and CUNDALL, 1998).

The model will of course never exactly match the observations made underground owing to the many simplifications and assumptions inherent in the model (including the assumption that a 2-D model can replicate a 3-D process). Also, due to the random nature of the models (and indeed the actual rock), the exact nature of the earthquake dynamics will be different each time a model is run, therefore direct comparisons with certain aspects of the recorded data is not always enlightening. However, it is hoped that the model can highlight some of the possible mechanisms and complexities associated with induced seismicity and unstable shear-slip events. More accurate models could be created in three dimensions such that the entire excavation is considered, however this would involve tremendous computer power and is beyond the scope of the present work.

Although this model represents small-scale microseismicity on a relatively small fault, it is thought that these types of discontinuum models could be scaled up to represent tectonic-scale earthquakes so that large-scale earthquake processes could be examined in detail. Simple particle models of the San Andreas fault have already

been created to try and explain the heat flow paradox (MORA and PLACE, 1998; SCOTT, 1996). If these models were run in a fully dynamic way with realistic levels of numerical damping (attenuation) it is possible that a variety of earthquake source information could be obtained from the models. In particular, a more detailed study of how dynamic triggering can contribute to event complexity, or even to remote triggering of other earthquakes would be of great interest (see HARRIS, 1998).

Conclusions

The excavation of a tunnel at Atomic Energy of Canada Ltd.'s Underground Research Laboratory has yielded many induced microseismic events. Because the microseismicity was recorded on two different scales (ultrasonic AE and lower frequency MS) it was thought that these events would provide a unique opportunity to examine the complexities of unstable shear slip in a brittle rock (granite). Several MS events associated with AE clusters have been thoroughly examined in COLLINS *et al.* (2002). To complement the seismic studies, a bonded-particle discontinuum model of one of the recorded AE clusters was created.

The model showed how the MS event was preceded by many small "foreshocks" and then followed by several discrete "aftershocks", exactly as observed underground. In addition, it was shown that the MS events themselves are quite complex. The model showed that slip on the fault was preceded by the formation of many small tensile cracks that facilitated slip between unbonded grains. The cracking/slip started at one point on the fault and propagated outwards at a finite speed until slip was occurring along the entire fault. In addition it was shown that the dynamic waves emitted by the tiny tensile cracks may have dynamically triggered other cracks on the fault, thereby adding to the complexity of the macro-fault slip.

AE and MS events produced by the model exhibited moment magnitudes about an order of magnitude larger than those actually recorded at the TSX. Possible reasons for this are that the complexity of the modelled events meant that the moment magnitude equations were inappropriately applied, and that the PFC events may not be dissipating enough energy during fracture formation and sliding. However, the dominant reason is probably that the shear strain was directly applied in the model causing fairly large magnitude events, whereas in the actual underground experiment it is likely that very small stress perturbations or a temporal decrease in rock strength triggered the recorded AE and MS events.

Future work will involve a more realistic simulation of the geometry and stress conditions around the TSX tunnel to endeavor to more accurately reproduce and explain the observed seismicity. In addition, future models could be scaled up to represent tectonic scale earthquakes and these models could be used as an attempt to answer some of the fundamental questions associated with earthquake dynamics and prediction.

Acknowledgements

We wish to thank David Lockner and another anonymous reviewer whose suggestions significantly improved the manuscript. This research was made possible by funding from the European Union under the INCO-Copernicus programme.

References

ANTONELLINI, M. A. and POLLARD, D. D. (1995), *Distinct Element Modeling of Deformation Bands in Sandstone*, J. Struct. Geology *17*, 1165–1182.

BAKER, C. and YOUNG, R. P. (1997), *Evidence for Extensile Crack Initiation in Point Source Time-dependent Moment Tensor Solutions*, Bull. Seismol. Soc. Am. *87*, 1442–1453.

BRACE, W. F. and BYERLEE, J. D. (1966), *Stick Slip as a Mechanism for Earthquakes*, Science *153*, 990–992.

BREHM, D. J. and BRAILE, L. W. (1998), *Intermediate-term Earthquake Prediction Using Precursory Events in the New Madrid Seismic Zone*, Bull. Seismol. Soc. Am. *88*, 564–580.

COLLINS, D. S. and YOUNG, R. P. (2000), *Lithological Controls on Seismicity in Granitic Rocks*, Bull. Seismol. Soc. Am. *90*, 709–723.

COLLINS, D. S. and YOUNG, R. P., *Acoustic emission and microseismic data from the excavation phase of the tunnel sealing experiment*. Report to Atomic Energy of Canada Limited, TSX-RP040 (Keele University, 1998).

COLLINS, D. S., PETTITT, W. S., and YOUNG, R. P. (2002), *High Resolution Mechanics of a Microearthquake Sequence*, Pure appl. geophys., *this issue*.

CUNDALL, P.A., *Numerical experiments on rough joints in shear using a bonded particle model*. In *Aspects of Tectonic Faulting* (eds. Lehner, F. K. and Urai, J. L.) (Springer-Verlag, Berlin 1999) pp. 1–10.

CUNDALL, P. A. and STRACK, O. (1979), *A Discrete Element Model for Granular Assemblies*, Geotechnique *29*, 47–65.

DAS, S. and SCHOLZ, C. H. (1981), *Theory of Time-dependent Rupture in the Earth*, J. Geophys. Res. *86*, 6039–6051.

FEUSTEL, A. J. (1995), *Seismic Attenuation in Underground Mines: Measurement Techniques and Applications to Site Characterization*, Ph.D. Thesis, Queen's University, Kingston, Ontario, Canada.

HARRIS, R. A. (1998), *Introduction to Special Session: Stress Triggers, Stress Shadows, and Implications for Seismic Hazard*, J. Geophys. Res. *103*, 24,347–24,358.

HAZZARD, J. F. and YOUNG, R. P. (2000), Simulating Acoustic Emissions in Bonded-Particle Models of Rock, Int. J. Rock Mech. Min. Sci. *37*, 867–872.

HAZZARD, J. F., YOUNG, R. P., and MAXWELL, S. C. (2000), *Micromechanical modelling of cracking and failure in brittle rocks*, J. Geophys. Res. *105*, 16,683–16,697.

ITASCA CONSULTING GROUP, *Particle Flow Code in 2 Dimensions* (Itasca Consulting Group, Minneapolis, 1999).

LOCKNER, D. A. (1998), *A Generalized Law for Brittle Deformation of Westerly Granite*, J. Geophys. Res. *103*, 5107–5123.

LOCKNER, D. A. (1993), *The Role of Acoustic Emission in the Study of Rock Fracture*, Int. J. Rock Mech. Min. Sci. and Geomech. Abstr. *30*, 883–899.

MCGARR, A. (1994), *Some Comparisons between Mining-Induced and Laboratory Earthquakes*, Pure Appl. Geophys. *142*, 467–489.

MORA, P. and PLACE, D. (1998), *Numerical Simulation of Earthquake Faults with Gouge: Toward a Comprehensive Explanation for the Heat Flow Paradox*, J. Geophys. Res. *103*, 21,067–21,089.

MORGAN, J. and BOETTCHER, M. S. (1999), *Numerical Simulations of Granular Shear Zones Using the Distinct Element Method 1. Shear Zone Kinematics and the micromechanics of localization*, J. Geophys. Res. *104*, 2703–2719.

PETTITT, W. S. (1998), *Acoustic Emission Source Studies of Microcracking in Rock*, Ph.D. Thesis, Keele University, Staffordshire, UK.

POTYONDY, D. O. and CUNDALL, P. A. (1998), *Modeling notch-formation mechanisms in the URL mine-by test tunnel using bonded assemblies of circular particles*, Int. J. Rock Mech. Min. Sci., Special Issue (Proceedings of NARMS '98, 3rd North American Rock Mechanics Symposium, Cancun, Mexico, June/July 1998), *35*, Paper no. 067, 1998.

POTYONDY, D. O. and CUNDALL, P. A. (1999), *Modeling of notch formation in the URL mine-by tunnel: Phase IV – Enhancements to the PFC model of rock*, Report to Atomic Energy of Canada Ltd. by Itasca Consulting Group, Minneapolis, issued as Ontario Hydro report No. 06819-REP-01200-10002-R00.

POTYONDY, D. O., CUNDALL, P. A., and LEE, C., *Modeling of rock using bonded assemblies of circular particles*. In *Second North American Rock Mechanics Symposium – NARMS '96* (ed. Aubertin, M.) (Balkema, Rotterdam, 1996) pp. 1934–1944.

SCHMIDTKE, R. H. and LAJTAI, E. Z. (1985), The Long-term Strength of Lac du Bonnet Granite, Int. J. Rock Mech. Min. Sci. & Geomech. Abstr. *22*(6), 461–465.

SCHOLZ, C. H., *The Mechanics of Earthquakes and Faulting* (Cambridge University Press, Cambridge, 1990).

SCOTT, D. R. (1996), *Seismicity and Stress Rotation in a Granular Model of the Brittle Crust*, Nature *381*, 592–595.

TAPPONNIER, P. and BRACE, W. F. (1976), *Development of Stress-induced Microcracks in Westerly Granite*, Int. J. Rock Mech. Min. Sci. Abstr. *13*, 103–112.

(Received April 4, 2000, revised/accepted August 10, 2000)